Global/local analytical and numerical free vibration analysis of sandwich columns

Zhengping Sun[a], Philippe Le Grognec[b,*], Kahina Sad Saoud[c]

[a] *Mines Douai, Polymers and Composites Technology & Mechanical Engineering Department, 941 rue Charles Bourseul, CS 10838, F-59508 Douai Cedex, France*
[b] *ENSTA Bretagne, UMR CNRS 6027, IRDL, F-29200 Brest, France*
[c] *Université de Sherbrooke, Department of Civil and Building Engineering, 2500 boulevard de l'Université, Sherbrooke, QC J1K 2R1, Canada*

Abstract

Sandwich structures are increasingly applied in many industrial fields of application, due to their lightweight combined with favorable mechanical properties. Despite this, such structures are subject to specific failure modes, such as buckling or vibratory resonance. In both cases, due to the presence of thin and stiff skins, global but also local modes may be of great interest when dimensioning such composite structures, which makes it impossible to use classical models. In this paper, the free vibration problem of classical sandwich columns (with homogeneous core materials) is investigated, using special kinematic models, so as to deal with both global and local eigenmodes in an effective and precise way. First, the problem is addressed analytically, where the two faces are represented by Euler-Bernoulli beams and the core material is considered as a 2D continuous solid, in small strain elasticity. Then, an enriched 1D finite element formulation is developed, so as to handle efficiently more general configurations encountered in practice. The homogeneous core layer is here described using hyperbolic functions, in accordance with the modal displacement fields obtained analytically. The present analytical and numerical solutions (natural frequencies and vibration modes) are contrasted against each other and compared to 2D reference numerical results.

Keywords: Sandwich structures, Modal analysis, Analytical modeling, Enriched finite element, Global/local vibration modes

1. Introduction

Classical sandwich structures are usually composed of two thin and stiff skin layers which are separated by a (homogeneous) much thicker and softer core layer. The strong mechanical properties (stemming from the stiffness of the skin layers and their distance to the middle surface of the composite) and the extreme lightweight (due to the low-density core material) of such composite materials, at the same time, make them

*Corresponding author.
Email address: philippe.le_grognec@ensta-bretagne.fr (Philippe Le Grognec)

particularly attractive in many applications, related to aerospace, marine or automotive industries, among others. In spite of these benefits, sandwich materials suffer from several weaknesses, mostly inherent to their heterogeneous structure. In practice, the buckling and vibration phenomena are among the most affected by the intrinsic nature of sandwich composites. In both situations, local modes, that are traditionally ignored in the analysis of homogeneous structures, shall be addressed here with sandwich materials, as they may occur before or shortly after the global ones (namely they may display similar critical values or eigenfrequencies). This increased emphasis on local modes has motivated one to develop specific advanced models, since standard 2D/3D models are clearly too onerous, and conventional beam/plate models are no longer suitable for the investigation of such local modes with relatively high wave numbers (or small wavelengths).

For about seventy years, numerous analytical and numerical sandwich models characterized by different levels of approximation have been defined in the literature. These models are mainly based on either Equivalent Single-Layer (ESL) or Layer-Wise (LW) theories, more broadly devoted to laminated composites, according to whether the kinematic fields are described in a global or discrete way. In ESL theories, emphasis is given to the enrichment of the in-plane displacements (using various non-linear functions) so as to reproduce the shear distribution as accurately as possible, giving rise to the so-called Higher-order/Refined Shear Deformation Theories. For a detailed literature review on ESL theories, the interested reader may refer to Reddy [1] and Carrera [2], for instance. In contrast, LW theories rely on piecewise displacement fields, which offer a more realistic representation of the composite through-thickness kinematics. Further details on such models, possibly involving the so-called zig-zag theory, and on the more advanced Carrera's/Generalized Unified Formulations may be found for instance in [3, 4]. Benchmark analyses of many theories and models are also gathered in the review articles by Liu and Li [5], Ghugal and Shimpi [6], Zhen and Wanji [7] and Hu et al. [8].

Besides, some specific models have been developed in the particular context of sandwich structures, like the so-called high-order sandwich panel theory (assuming uniform shear in the core thickness), and the extended high-order sandwich panel theory (also including the in-plane rigidity of the core material) which has been thoroughly examined in the framework of static and buckling analyses by Phan et al. [9, 10], among others. More specifically, many authors have tried to formulate unified models capable of describing both global and local modes (both symmetric and antisymmetric). The buckling problem has probably received the greatest attention, since the pioneering works from Allen [11] and Benson and Mayers [12]. Conversely, the problem of free vibrations of sandwich columns was less studied. From an analytical point of view, Sakiyama et al. [13] investigated the free vibration problem of a three-layer sandwich beam (possibly non-symmetric) with a visco-elastic core material by applying the Green function method, but considered classical beam kinematics for the three layers, including the core. Banerjee and Sobey [14] implemented the so-called dynamic stiffness theory in order to calculate the natural frequencies and mode shapes of three-

layer sandwich beams, where the skin and core layers were described using Rayleigh and Timoshenko beam models, respectively. Later on, Banerjee et al. [15] improved the previous model by replacing the Rayleigh beam model by a Timoshenko beam model for each skin layer (the core being still represented by the same Timoshenko beam model), and they performed experiments so as to validate their theoretical results. Lou et al. [16] analyzed the free vibrations of sandwich beams with lattice truss core. In their study, the pyramidal truss core is homogenized into a continuous material of which only the shear response (which is supposed to be uniform in the thickness direction) is taken into account. Dealing now with sandwich plates, Kant and Swaminathan [17] solved analytically the problem of free vibration using a refined theory (also suitable for laminates) based on polynomial displacement fields defined through the whole plate thickness. Alternatively, the vibration problem of sandwich beams has been widely studied from a numerical point of view using, most of the time, the finite element method. As an example, Arvin et al. [18] performed a numerical study of the free and forced vibrations of a sandwich beam with composite faces and a visco-elastic core material, using linear kinematics through the core thickness. Furthermore, let us cite Wang and Wang [19] who recently used the weak form quadrature element method so as to deal with the free vibration analysis of soft-core sandwich beams. The skins were modeled as Euler-Bernoulli beams whereas a higher-order beam formulation was used for the description of the core layer. As a continuation of this work, Wang and Liang [20] extended the previous model to a 2D continuous representation of the core layer, by no longer using a 1D but a 2D quadrature element method, what allowed them to predict also more complex modes such as symmetric ones, but in a less efficient way. Except in the latter case, all the models presented above are generally not appropriate for an accurate determination of the whole set of natural frequencies and corresponding modes of sandwich columns, notably in the case of thick and soft core layers that may deform "two-dimensionally" instead of in the same way as a beam. Particularly, many modes (among which symmetric ones) may not (or only poorly) be described by most of the previous models.

The present paper deals with the free vibrations of sandwich columns. First, the problem is solved analytically, by means of Hamilton's principle. At first sight, the vibration response of a sandwich material can be seen as the vibration of one (or both) face(s) on either side of the homogeneous core layer. However, despite its comparatively low modulus and density, the core material strongly influences both the natural frequencies and the corresponding vibration modes of the sandwich structure. Special attention must thus be paid to the core material representation so as to estimate the vibration response with a good accuracy, including the possible interaction between the two skins. In our approach, the main improvement beside previous models arises from the absence of specific hypotheses for the core kinematics. While the faces are classically considered as slender beams, the foam core is represented by a 2D continuous solid, without any simplification regarding the deformation field, as has been already done in [21] in the case of buckling. Using such kinematics, a set of partial differential equations is obtained, which is solved for given classical boundary conditions, giving rise to original analytical solutions of the eigenfrequencies and associated eigenmodes.

Secondly, as closed-form solutions are usually not available in practical situations, a specific 1D beam-like finite element model has been previously developed first in the context of elastic linearized buckling [22], which turns out to be an efficient numerical tool for dimensioning purposes of sandwich columns, when compared to a classical 2D finite element model. This enriched finite element is here enhanced so as to deal with the dynamic response of sandwich columns (a special emphasis will be placed on the construction of the mass matrix, which is really new). The same kinematics as before are retained, according to the fact that nearly the same expressions are obtained analytically in both contexts of buckling and vibration, in terms of modal displacement shapes with respect to the core thickness position. Therefore, while the skins are here typically modeled by Timoshenko beams, the displacement fields in the core layer are defined as hyperbolic functions of the through-thickness parameter. The original finite element formulation is implemented in a bespoke Fortran program, that allows one to perform a modal analysis and derive the eigenfrequencies and corresponding eigenmodes of any sandwich column with arbitrary boundary conditions, in a robust and efficient way.

The present analytical and numerical results are contrasted against each other and compared to reference numerical results, obtained through classical 2D finite element computations (linearized frequency analyses) using Abaqus software, for validation purposes. It is shown that, in the case of a particularly thick and soft core layer, the natural frequencies corresponding to the global and local modes may be of the same order of magnitude. Local modes must be therefore considered with interest and are demonstrated to be accurately, and yet efficiently, predicted with such modeling approaches. In particular, as far as symmetric modes are concerned, for each wave number characterizing the sinusoidal modal deformation shape of the faces, two distinct modes are revealed with different modal fields inside the core layer and different natural frequencies, which constitutes a new finding to the best of the authors' knowledge.

2. Analytical modeling of the free vibration behavior of sandwich columns

2.1. Problem definition

Let us consider a symmetric sandwich column with homogeneous skin and core materials (the two skins are thus supposed to be identical, like in most practical cases). A 2D representation of the sandwich column (in the xy-plane) is retained with a unit depth (in the z-direction). The total length of the sandwich structure (along the x-axis) is denoted by L, whereas the thicknesses of the foam core and the two skins (along the y-direction) are respectively $2h_c$ and $2h_s$ (see Figure 1).

The following assumptions are made so as to simplify the analysis. The facings are assumed to behave like Euler-Bernoulli beams. Transverse shear effects are neglected due to their low thickness-to-length ratios. Moreover, as far as motion equations are concerned, the rotational inertia terms are also neglected, as well as the longitudinal average acceleration terms (related to the centroid axes), in such a way that the kinetic

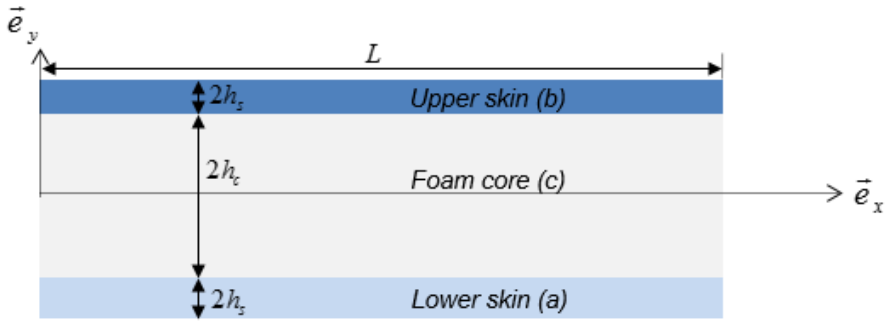


Figure 1: Two-dimensional representation of the sandwich column

energy of both skins only involves the transverse displacement rate of each of them. Conversely, the foam core is modeled here as a 2D continuous solid satisfying the plane stress hypothesis. The isotropic foam core is supposed to be linearly elastic (with Young's modulus E_c and Poisson's ratio ν_c). As for the two elastic skins, due to the kinematic hypotheses, only their Young's modulus E_s will be involved subsequently. The mass per unit volume of the skin and core materials is ρ_s and ρ_c, respectively. Only small displacements and strains are considered throughout the paper.

2.2. Theoretical formulation

The problem of free vibration of a sandwich column can be formulated using Hamilton's principle:

$$\int_{t_1}^{t_2} (\delta T - \delta U) \mathrm{d}t = 0 \tag{1}$$

The total elastic energy U of the sandwich column can be viewed as the sum of the elastic strain energies of the three layers:

$$U = \sum_{i=a,b,c} \frac{1}{2} \int_{\Omega_i} \boldsymbol{\sigma}_i : \boldsymbol{\varepsilon}_i \mathrm{d}\Omega \tag{2}$$

whereas the total kinetic energy T writes similarly:

$$T = \sum_{i=a,b,c} \frac{1}{2} \int_{\Omega_i} \rho_i \dot{\mathbf{u}}_i . \dot{\mathbf{u}}_i \mathrm{d}\Omega \tag{3}$$

where the dot denotes the differentiation with respect to time t.

On one side, both skins are represented by Euler-Bernoulli beams, as transverse shear effects may be negligible in practice. As far as the bending problem in the xy-plane is concerned, the Euler-Bernoulli kinematics is defined by two scalar displacement fields $u_i(x,t)$ and $v_i(x,t)$ (for $i = a$ or b, depending on the skin considered), respectively the axial and transverse displacements of the centroid axis of the beam. The general displacement field of a current point of a skin writes then in the orthonormal basis $(\mathbf{e}_x, \mathbf{e}_y, \mathbf{e}_z)$:

$$\mathbf{u}_i = \left| \begin{array}{l} u_i - y v_{i,x} \\ v_i \\ 0 5 \end{array} \right. \tag{4}$$

where y denotes the through-thickness position with respect to the centroid axis of the considered beam.

Therefore, the strain and stress tensors, respectively denoted by $\boldsymbol{\varepsilon}_i$ and $\boldsymbol{\sigma}_i$ for each skin $i = a, b$, take the following form in the same orthonormal basis, only involving the Young's modulus due to the uniaxial stress state:

$$\boldsymbol{\varepsilon}_i = \begin{bmatrix} u_{i,x} - y v_{i,xx} & 0 & 0 \\ 0 & 0 & 0 \\ 0 & 0 & 0 \end{bmatrix} \qquad \boldsymbol{\sigma}_i = \begin{bmatrix} E_s(u_{i,x} - y v_{i,xx}) & 0 & 0 \\ 0 & 0 & 0 \\ 0 & 0 & 0 \end{bmatrix} \tag{5}$$

On the other side, the displacement field in the core layer does not rely on particular kinematics and takes thus the general following form (in 2D):

$$\mathbf{u}_c = \begin{vmatrix} u_c \\ v_c \\ 0 \end{vmatrix} \tag{6}$$

where $u_c(x, y, t)$ and $v_c(x, y, t)$ represent the longitudinal and transverse displacement components, respectively.

The present 2D model is supposed to reproduce the behavior of a sandwich column with small lateral dimensions, so that the plane stress hypothesis is adopted. The strain and stress tensors in the core layer can then be deduced as follows, involving the appropriate reduced moduli:

$$\begin{aligned} \boldsymbol{\varepsilon}_c &= \begin{bmatrix} u_{c,x} & \frac{1}{2}(u_{c,y} + v_{c,x}) & 0 \\ \frac{1}{2}(u_{c,y} + v_{c,x}) & v_{c,y} & 0 \\ 0 & 0 & 0 \end{bmatrix} \\ \boldsymbol{\sigma}_c &= \begin{bmatrix} (\lambda_c^* + 2\mu_c) u_{c,x} + \lambda_c^* v_{c,y} & \mu_c(u_{c,y} + v_{c,x}) & 0 \\ \mu_c(u_{c,y} + v_{c,x}) & \lambda_c^* u_{c,x} + (\lambda_c^* + 2\mu_c) v_{c,y} & 0 \\ 0 & 0 & 0 \end{bmatrix} \end{aligned} \tag{7}$$

with $\lambda_c^* = \frac{2\lambda_c \mu_c}{\lambda_c + 2\mu_c}$ (λ_c and μ_c are the Lamé constants related to E_c and ν_c by the standard relations $\lambda_c = \frac{E_c \nu_c}{(1+\nu_c)(1-2\nu_c)}$ and $\mu_c = \frac{E_c}{2(1+\nu_c)}$).

After integration through the thickness of each skin layer, the total strain energy of the whole sandwich becomes:

$$\begin{aligned} U = \; & \textstyle\sum_{i=a,b} \frac{1}{2} \int_0^L \left(2E_s h_s u_{i,x}^{\,2} + \frac{2E_s h_s^3}{3} v_{i,xx}^{\,2} \right) \mathrm{d}x \\ & + \frac{1}{2} \int_{\Omega_c} \left[(\lambda_c^* + 2\mu_c) u_{c,x}^{\,2} + 2\lambda_c^* u_{c,x}\, v_{c,y} + (\lambda_c^* + 2\mu_c) v_{c,y}^{\,2} + \mu_c u_{c,y}^{\,2} + 2\mu_c u_{c,y}\, v_{c,x} + \mu_c v_{c,x}^{\,2} \right] \mathrm{d}\Omega \end{aligned} \tag{8}$$

whereas the total kinetic energy T of the sandwich column simply writes as follows, due to the preceding assumptions:

$$T = \sum_{i=a,b} \frac{1}{2} \int_0^L 2\rho_s h_s \dot{v}_i^2 \mathrm{d}x + \frac{1}{2} \int_{\Omega_c} \rho_c (\dot{u}_c^2 + \dot{v}_c^2) \mathrm{d}\Omega \tag{9}$$

One can then express Hamilton's principle (Equation (1)) in the following way, by differentiating the above two energies:

$$\begin{aligned}
&\int_{t_1}^{t_2} \Big(\textstyle\sum_{i=a,b} \int_0^L 2\rho_s h_s \dot{v}_i \delta\dot{v}_i \mathrm{d}x + \int_{\Omega_c} \rho_c (\dot{u}_c \delta\dot{u}_c + \dot{v}_c \delta\dot{v}_c) \mathrm{d}\Omega \\
&\quad - \textstyle\sum_{i=a,b} \int_0^L \Big(2E_s h_s u_{i,x}\, \delta u_{i,x} + \frac{2E_s h_s^3}{3} v_{i,xx}\, \delta v_{i,xx} \Big) \mathrm{d}x \\
&\quad - \int_{\Omega_c} [(\lambda_c^* + 2\mu_c) u_{c,x}\, \delta u_{c,x} + \lambda_c^* u_{c,x}\, \delta v_{c,y} + \lambda_c^* v_{c,y}\, \delta u_{c,x} \\
&+ (\lambda_c^* + 2\mu_c) v_{c,y}\, \delta v_{c,y} + \mu_c u_{c,y}\, \delta u_{c,y} + \mu_c u_{c,y}\, \delta v_{c,x} + \mu_c v_{c,x}\, \delta u_{c,y} + \mu_c v_{c,x}\, \delta v_{c,x}]\, \mathrm{d}\Omega \big)\, \mathrm{d}t = 0
\end{aligned} \tag{10}$$

After integration by parts with respect to x, y and t, it should be noted that the variations δu_i and δv_i (for $i = a, b, c$) must vanish at the bounds of integration t_1 and t_2 according to Hamilton's principle. Furthermore, since all these variations are arbitrary, the following partial differential equations of motion (in free vibrations) can be deduced:

$$2E_s h_s u_{a,xx} + \mu_c \, (u_{c,y} + v_{c,x}) \big|_{y=-h_c} = 0 \tag{11}$$

$$\frac{2E_s h_s^3}{3} v_{a,xxxx} - \lambda_c^* \, u_{c,x} \big|_{y=-h_c} - (\lambda_c^* + 2\mu_c) \, v_{c,y} \big|_{y=-h_c} - h_s \mu_c \, (u_{c,xy} + v_{c,xx}) \big|_{y=-h_c} + 2\rho_s h_s \ddot{v}_a = 0 \tag{12}$$

$$2E_s h_s u_{b,xx} - \mu_c \, (u_{c,y} + v_{c,x}) \big|_{y=h_c} = 0 \tag{13}$$

$$\frac{2E_s h_s^3}{3} v_{a,xxxx} + \lambda_c^* \, u_{c,x} \big|_{y=h_c} + (\lambda_c^* + 2\mu_c) \, v_{c,y} \big|_{y=h_c} - h_s \mu_c \, (u_{c,xy} + v_{c,xx}) \big|_{y=h_c} + 2\rho_s h_s \ddot{v}_b = 0 \tag{14}$$

$$(\lambda_c^* + 2\mu_c) u_{c,xx} + \mu_c u_{c,yy} + (\lambda_c^* + \mu_c) v_{c,xy} - \rho_c \ddot{u}_c = 0 \tag{15}$$

$$(\lambda_c^* + 2\mu_c) v_{c,yy} + \mu_c v_{c,xx} + (\lambda_c^* + \mu_c) u_{c,xy} - \rho_c \ddot{v}_c = 0 \tag{16}$$

The last two equations (15) and (16) identify with classical motion equations of the core region in a 2D framework. Conversely, the first four equations (11), (12), (13) and (14) look like classical equations for beams, but also include additional terms (naturally obtained through integrations by parts) characterizing the influence of the core layer on the dynamic response of the skins.

At this stage, one has to specify the boundary conditions in order to solve the previous system. First, connecting conditions for the displacement fields must be satisfied at the interfaces between the foam core and the two facings, namely:

$$\forall x \in]0, L[, \qquad \begin{aligned} &u_a - h_s v_{a,x} - u_c|_{y=-h_c} = 0 \\ &u_b + h_s v_{b,x} - u_c|_{y=h_c} = 0 \\ &v_a - v_c|_{y=-h_c} = 0 \\ &v_b - v_c|_{y=h_c} = 0 \end{aligned} \tag{17}$$

In the sequel, the free vibration problem will be mainly investigated in the case of a sandwich beam guided at both ends, considering thus the same boundary conditions as in the buckling analysis performed in [21]. These conditions have been retained as they lead to closed-form expressions for the eigenmodes as far as single beams are concerned. Let us mention that very similar solutions may be obtained in the case of a simply-supported sandwich beam, for instance. In the present case, the two ends of each face act as if they were guided, what leads to the following kinematical constraints: $u_a(0,t) = u_a(L,t) = u_b(0,t) = u_b(L,t) = 0$ and $v_{a,x}(0,t) = v_{a,x}(L,t) = v_{b,x}(0,t) = v_{b,x}(L,t) = 0$. Taking into account $\delta u_a(0) = \delta u_a(L) = \delta u_b(0) = \delta u_b(L) = 0$ and $\delta v_{a,x}(0) = \delta v_{a,x}(L) = \delta v_{b,x}(0) = \delta v_{b,x}(L) = 0$ in Equation (10) leads one, after integration by parts, to the remaining natural boundary conditions for the skins:

$$\begin{array}{l} \frac{2E_s h_s^3}{3} v_{a,xxx}(0,t) - h_s \mu_c \left(u_{c,y}(0,-h_c,t) + v_{c,x}(0,-h_c,t)\right) = 0 \\ \frac{2E_s h_s^3}{3} v_{a,xxx}(L,t) - h_s \mu_c \left(u_{c,y}(L,-h_c,t) + v_{c,x}(L,-h_c,t)\right) = 0 \\ \frac{2E_s h_s^3}{3} v_{b,xxx}(0,t) - h_s \mu_c \left(u_{c,y}(0,h_c,t) + v_{c,x}(0,h_c,t)\right) = 0 \\ \frac{2E_s h_s^3}{3} v_{b,xxx}(L,t) - h_s \mu_c \left(u_{c,y}(L,h_c,t) + v_{c,x}(L,h_c,t)\right) = 0 \end{array} \tag{18}$$

The last boundary conditions refer to the two remaining edges of the foam zone. Displacement boundary conditions are also enforced in the axial direction at $x = 0$ and $x = L$, that is to say:

$$\forall y \in]-h_c, h_c[, \qquad \begin{array}{l} u_c|_{x=0} = 0 \\ u_c|_{x=L} = 0 \end{array} \tag{19}$$

Since these two edges are free in the y-direction, the last two equations consist in the following stress boundary conditions:

$$\forall y \in]-h_c, h_c[, \qquad \begin{array}{l} \mu_c \left(u_{c,y} + v_{c,x}\right)|_{x=0} = 0 \\ \mu_c \left(u_{c,y} + v_{c,x}\right)|_{x=L} = 0 \end{array} \tag{20}$$

2.3. Solution procedure

According to the method of separation of variables, the general solution of Equations (11-16) is assumed to take the following form:

$$\left\{ \begin{array}{l} u_a(x,t) = \sum_n u_{a(n)}(x)\varphi_n(t) \\ u_b(x,t) = \sum_n u_{b(n)}(x)\varphi_n(t) \\ v_a(x,t) = \sum_n v_{a(n)}(x)\varphi_n(t) \\ v_b(x,t) = \sum_n v_{b(n)}(x)\varphi_n(t) \\ u_c(x,y,t) = \sum_n u_{c(n)}(x,y)\varphi_n(t) \\ v_c(x,y,t) = \sum_n v_{c(n)}(x,y)\varphi_n(t) \end{array} \right. \tag{21}$$

Functions $u_{a(n)}$, $u_{b(n)}$, $v_{a(n)}$, $v_{b(n)}$, $u_{c(n)}$ and $v_{c(n)}$ represent the components of the sought eigenmodes, whereas φ_n is the associated time function which may write, in the context of harmonic vibrations:

$$\varphi_n(t) = e^{\mathrm{i}\omega t} \tag{22}$$

where ω stands for the eigenfrequency corresponding to eigenmode "n".

The frequency modes of a single Euler-Bernoulli beam with the boundary conditions defined above take the following form:

$$\begin{cases} u = 0 \\ v = \cos \frac{n\pi x}{L} \end{cases} \tag{23}$$

where $n \in \mathbb{N}^*$ is the associated half-wave number. According to Equation (23) and preliminary numerical observations, the following assumptions are made for the skin components of the frequency modes of the sandwich column:

$$\begin{cases} u_{a(n)} = \alpha \sin \frac{n\pi x}{L} \\ u_{b(n)} = \pm\alpha \sin \frac{n\pi x}{L} \\ v_{a(n)} = \cos \frac{n\pi x}{L} \\ v_{b(n)} = \pm \cos \frac{n\pi x}{L} \end{cases} \tag{24}$$

The components $v_{a(n)}$ and $v_{b(n)}$ are identical to the corresponding one in Equation (23), assuming that the core layer does not alter the transverse modal displacement shape. Owing to the symmetry of the sandwich column, the same unit amplitude is retained for both faces. However, two cases are considered, depending on the relative sign of the two fields $v_{a(n)}$ and $v_{b(n)}$. The vibration mode of the sandwich column may thus be antisymmetric ($v_{b(n)} = v_{a(n)}$) or symmetric ($v_{b(n)} = -v_{a(n)}$). Conversely, the longitudinal components $u_{a(n)}$ and $u_{b(n)}$ are no longer zero as in the case of a single beam due to the presence of the foam on one side only. A sinusoidal shape is also retained for these components, which is consistent with the associated boundary conditions, together with an unknown amplitude α to be determined and a possible different sign between them (in practice, $u_{b(n)} = u_{a(n)}$ when considering a symmetric mode and $u_{b(n)} = -u_{a(n)}$ for an antisymmetric mode).

Concerning the foam core modal displacement fields, a separation of spatial variables is also performed and the following forms are presupposed, according to Equation (24):

$$\begin{cases} u_{c(n)} = \zeta(y) \sin \frac{n\pi x}{L} \\ v_{c(n)} = \eta(y) \cos \frac{n\pi x}{L} \end{cases} \tag{25}$$

The modal displacement fields (24) and (25) are such that all the boundary conditions at $x = 0$ and $x = L$ are automatically verified.

2.3.1. Antisymmetric case

In order to find the antisymmetric modes and corresponding eigenvalues, the following expressions are introduced in Equations (11-20):

$$\begin{cases} u_a = \alpha \sin \frac{n\pi x}{L} e^{\mathrm{i}\omega t} \\ u_b = -\alpha \sin \frac{n\pi x}{L} e^{\mathrm{i}\omega t} \\ v_a = \cos \frac{n\pi x}{L} e^{\mathrm{i}\omega t} \\ v_b = \cos \frac{n\pi x}{L} e^{\mathrm{i}\omega t} \\ u_c = \zeta(y) \sin \frac{n\pi x}{L} e^{\mathrm{i}\omega t} \\ v_c = \eta(y) \cos \frac{n\pi x}{L} e^{\mathrm{i}\omega t} \end{cases} \tag{26}$$

Equations (15) and (16) simplify as follows:

$$\begin{aligned} &2\left(\omega^2\rho_c(\nu_c^2-1)L^2 + n^2\pi^2 E_c\right)\zeta + E_c L\left(L(nu_c-1)\zeta_{,yy} + n\pi(nu_c+1)\eta_{,y}\right) = 0 \\ &\left(2\omega^2\rho_c(\nu_c+1)L^2 - n^2\pi^2 E_c\right)(nu_c-1)\eta - E_c L\left(2L\eta_{,yy} + n\pi(nu_c+1)\zeta_{,y}\right) = 0 \end{aligned} \tag{27}$$

and the four connecting conditions (17) become:

$$\begin{aligned} &\alpha + \tfrac{n\pi h_s}{L} - \zeta(-h_c) = 0 \\ &1 - \eta(-h_c) = 0 \\ &\alpha + \tfrac{n\pi h_s}{L} + \zeta(h_c) = 0 \\ &1 - \eta(h_c) = 0 \end{aligned} \tag{28}$$

Equations (27) and (28) can be solved together, leading to the following solutions for functions ζ and η:

$$\begin{aligned} \zeta &= k_1 \sinh\left(\frac{\sqrt{n^2\pi^2 E_c - 2\omega^2\rho_c L^2(\nu_c+1)}\,y}{L\sqrt{E_c}}\right) + k_2 \sinh\left(\frac{\sqrt{n^2\pi^2 E_c - \omega^2\rho_c L^2(1-\nu_c^2)}\,y}{L\sqrt{E_c}}\right) \\ \eta &= k_3 \cosh\left(\frac{\sqrt{n^2\pi^2 E_c - 2\omega^2\rho_c L^2(\nu_c+1)}\,y}{L\sqrt{E_c}}\right) + k_4 \cosh\left(\frac{\sqrt{n^2\pi^2 E_c - \omega^2\rho_c L^2(1-\nu_c^2)}\,y}{L\sqrt{E_c}}\right) \end{aligned} \tag{29}$$

where k_1, k_2, k_3 and k_4 are constant coefficients whose expressions are too cumbersome to be written in this paper. Let us mention that in practice, whatever the integer n considered, the final eigenfrequency will generally be such that the arguments of the two square roots in Equation (29) are actually positive.

Then, Equation (11) (equivalent to Equation (13)) is solved in order to determine α:

$$4n^2\pi^2 E_s h_s \alpha(1+\nu_c) - E_c L\left(L\zeta_{,y}(\pm h_c) - n\pi\eta(\pm h_c)\right) = 0 \tag{30}$$

and Equation (12) (equivalent to Equation (14)), which is transcendental, is numerically solved so as to obtain finally the sought eigenfrequency ω:

$$\begin{aligned} &3n\pi E_c h_s L^3(\nu_c-1)\zeta_{,y}(\pm h_c) - 3n^2\pi^2 E_c h_s L^2(\nu_c-1)\eta(\pm h_c) - 6E_c L^4\eta_{,y}(\pm h_c) \\ &-6n\pi E_c\nu_c L^3\zeta(\pm h_c) - 4h_s(1-\nu_c^2)(3\omega^2\rho_s L^4 - n^4\pi^4 E_s h_s^2) = 0 \end{aligned} \tag{31}$$

2.3.2. Symmetric case

The case of symmetric modes is solved in a similar way. The expressions (26) are replaced here by:

$$\begin{cases} u_a = \alpha \sin \frac{n\pi x}{L} e^{\mathrm{i}\omega t} \\ u_b = \alpha \sin \frac{n\pi x}{L} e^{\mathrm{i}\omega t} \\ v_a = \cos \frac{n\pi x}{L} e^{\mathrm{i}\omega t} \\ v_b = -\cos \frac{n\pi x}{L} e^{\mathrm{i}\omega t} \\ u_c = \zeta(y) \sin \frac{n\pi x}{L} e^{\mathrm{i}\omega t} \\ v_c = \eta(y) \cos \frac{n\pi x}{L} e^{\mathrm{i}\omega t} \end{cases} \tag{32}$$

Introducing these new expressions in Equations (15) and (16) leads to the following general solutions:

$$\begin{aligned} \zeta &= k_1 \cosh\left(\frac{\sqrt{n^2\pi^2 E_c - 2\omega^2\rho_c L^2(\nu_c+1)}y}{L\sqrt{E_c}}\right) + k_2 \cosh\left(\frac{\sqrt{n^2\pi^2 E_c - \omega^2\rho_c L^2(1-\nu_c^2)}y}{L\sqrt{E_c}}\right) \\ \eta &= k_3 \sinh\left(\frac{\sqrt{n^2\pi^2 E_c - 2\omega^2\rho_c L^2(\nu_c+1)}y}{L\sqrt{E_c}}\right) + k_4 \sinh\left(\frac{\sqrt{n^2\pi^2 E_c - \omega^2\rho_c L^2(1-\nu_c^2)}y}{L\sqrt{E_c}}\right) \end{aligned} \tag{33}$$

In practice, due to the possible negative sign of $n^2\pi^2 E_c - 2\omega^2\rho_c L^2(\nu_c+1)$ and $n^2\pi^2 E_c - \omega^2\rho_c L^2(1-\nu_c^2)$, the hyperbolic functions in Equation (33) may be replaced by appropriate trigonometric functions so as to avoid expressions including any complex number. For example, in the extreme case where $n^2\pi^2 E_c - \omega^2\rho_c L^2(1-\nu_c^2) < 0$ (which implies $n^2\pi^2 E_c - 2\omega^2\rho_c L^2(\nu_c+1) < 0$), Equation (33) may be rewritten as follows:

$$\begin{aligned} \zeta &= k_1 \cos\left(\frac{\sqrt{-n^2\pi^2 E_c + 2\omega^2\rho_c L^2(\nu_c+1)}y}{L\sqrt{E_c}}\right) + k_2 \cos\left(\frac{\sqrt{-n^2\pi^2 E_c + \omega^2\rho_c L^2(1-\nu_c^2)}y}{L\sqrt{E_c}}\right) \\ \eta &= k_3 \sin\left(\frac{\sqrt{-n^2\pi^2 E_c + 2\omega^2\rho_c L^2(\nu_c+1)}y}{L\sqrt{E_c}}\right) + k_4 \sin\left(\frac{\sqrt{-n^2\pi^2 E_c + \omega^2\rho_c L^2(1-\nu_c^2)}y}{L\sqrt{E_c}}\right) \end{aligned} \tag{34}$$

In all cases, Equation (11) (or (13)) can be solved in order to determine α, and then Equation (12) (or (14)) is numerically solved so as to obtain the eigenfrequency ω. Conversely to the antisymmetric case where only one solution is obtained for each wave number n, the resolution of Equation (12) leads here to two different eigenfrequencies. It means that, as far as symmetric modes are concerned, for each sinusoidal modal deformed shape of the skins (for each given wave number), two different modes (modal deformed shapes of the core layer) may co-exist with two different associated frequencies, as will be seen later.

In the antisymmetric case, integer n is supposed to be strictly positive, as $n = 0$ would correspond to a rigid mode for the whole sandwich structure. In the symmetric case, $n = 0$ also corresponds to a rigid mode for both skins, when considered independently, but to a vibration mode (with a non null eigenfrequency) for the whole sandwich, due to the deformation of the core layer. This particular case is worthy of interest and will be thus presented in the sequel.

Inserting $n = 0$ in Equation (32) leads to the simplified following expressions:

$$\begin{cases} u_a = 0 \\ u_b = 0 \\ v_a = e^{\mathrm{i}\omega t} \\ v_b = -e^{\mathrm{i}\omega t} \\ u_c = 0 \\ v_c = \eta(y) e^{\mathrm{i}\omega t} \end{cases} \tag{35}$$

Equation (15) is automatically verified and Equation (16) simply writes:

$$E_c \eta_{,yy} + \omega^2 \rho_c (1 - \nu_c^2) \eta = 0 \tag{36}$$

The solution of Equation (36), considering the connecting conditions $\eta(-h_c) = 1$ and $\eta(h_c) = -1$, is as follows:

$$\eta = k \sin\left(\omega \sqrt{\frac{\rho_c (1 - \nu_c^2)}{E_c}} y \right) \tag{37}$$

with:

$$k = -\frac{1}{\sin\left(\omega \sqrt{\frac{\rho_c (1 - \nu_c^2)}{E_c}} h_c \right)} \tag{38}$$

Equations (11) and (13) are naturally satisfied and Equations (12) and (14), still transcendental:

$$E_c \eta_{,y}\left(\pm h_c\right) + 2\omega^2 \rho_s h_s (1 - \nu_c^2) = k\omega \sqrt{E_c \rho_c (1 - \nu_c^2)} \cos\left(\omega \sqrt{\frac{\rho_c (1 - \nu_c^2)}{E_c}} h_c \right) + 2\omega^2 \rho_s h_s (1 - \nu_c^2) = 0 \tag{39}$$

coincide and lead thus to the same eigenfrequency.

3. An enriched 1D finite element for the vibration analysis of sandwich columns

Hereafter, the vibration problem of a sandwich column is investigated from a numerical point of view, in order to deal more easily with various boundary conditions and, in the longer term, with more general (possibly non-linear) dynamics problems. For obvious efficiency purposes, it was decided to develop here a 1D enriched finite element model on the basis of what was done before by some of the authors in the context of buckling and post-buckling (see [22, 23] for more details on this subject). The main features of this so-called "sandwich beam" finite element will be first recalled here, limiting ourselves to a linear framework (since this study only deals with linear vibrations), and attention will be focused then on the new inertial terms which are naturally needed to perform linearized frequency analyses.

3.1. Kinematics and constitutive laws

The same geometric and material configuration is considered, as in the previous analytical section, and the same notations are used. Some specific kinematic assumptions are made for both the skin and core layers, which result in a proper representation of the through-thickness distribution of strain/stress fields.

3.1.1. Skin layers

Skin layers are represented by Timoshenko beams, accounting for transverse shear effects, making thus possible to deal with all kinds of sandwich columns including short ones. The displacement field in each face ($i = a, b$) may thus be expressed as follows, in the same (2D) coordinate system as before, according to Timoshenko kinematics:

$$\mathbf{u}^i(x, y, t) = \left| \begin{array}{l} u^i(x,t) - y\theta^i(x,t) \\ v^i(x,t) \end{array} \right. \tag{40}$$

where u^i and v^i are respectively the longitudinal and transverse displacements of the centroid axis of face i, and θ^i represents the rotation of its cross-section about the $\mathbf{e}_z$ axis, y being the transverse coordinate of a current point relative to its mid-axis.

The linearized Green strain tensor writes then:

$$\boldsymbol{\varepsilon}^i = \frac{1}{2}(\nabla \mathbf{u}^i + \nabla^T \mathbf{u}^i) \tag{41}$$

whose non-zero components may be compiled in a reduced vector:

$$\boldsymbol{\gamma}_i = \left\langle \varepsilon^i_{xx} \ , \ 2\varepsilon^i_{xy} \right\rangle^T = \left\langle u^{,i}_{x} - y\theta^{,i}_{x} \ , \ v^{,i}_{x} - \theta^i \right\rangle^T \tag{42}$$

Finally, in the case of an isotropic linear elastic material, according to the Hooke's law, the stress tensor writes:

$$\boldsymbol{\sigma}^i = \lambda_s tr(\boldsymbol{\varepsilon}^i)\mathbf{I} + 2\mu_s \boldsymbol{\varepsilon}^i \tag{43}$$

where λ_s and μ_s stand for the Lamé constants of the skin material, and $\mathbf{I}$ is the second-order unit tensor. Owing to the actual anti-plane stress state, only the two following non-zero stress components will be involved in the subsequent developments:

$$\mathbf{s}_i = \left\{ \begin{array}{c} \sigma^i_{xx} \\ \sigma^i_{xy} \end{array} \right\} = \left[\begin{array}{cc} E_s & 0 \\ 0 & \mu_s \end{array} \right] \left\{ \begin{array}{c} \varepsilon^i_{xx} \\ 2\varepsilon^i_{xy} \end{array} \right\} = \mathbf{L}_s \boldsymbol{\gamma}_i \tag{44}$$

3.1.2. Core layer

The kinematics used for the core layer is mainly based on hyperbolic functions which were deduced from analytical solutions obtained in the context of buckling analyses (this issue is discussed in depth in [21, 22]). These expressions are supposedly good approximations of functions ζ and η which describe here the evolution of the modal displacement fields in the core layer along the thickness, in the context of vibrations.

The displacement field within the core layer is therefore given by the following expressions:

$$\mathbf{u}^c(x,y,t) = \left| \begin{array}{l} u_0^c(x,t) + u_1^c(x,t)\sinh(\frac{\pi y}{L}) + f(x,y,t) \\ v_0^c(x,t)\cosh(\frac{\pi y}{L}) + v_1^c(x,t)y + g(x,y,t) \end{array} \right. \tag{45}$$

where y represents here the thickness coordinate relative to the mid-axis of the core layer.

The enrichment functions f and g in Equation (45), intended to describe the local effects that are likely to occur in the core layer, are defined as the following combinations of hyperbolic sine and cosine functions:

$$\left\{ \begin{array}{l} f(x,y,t) = \phi_1(x,t)\cosh(\alpha y) + \phi_2(x,t)\sinh(\alpha y) + \phi_3(x,t)y\cosh(\alpha y) + \phi_4(x,t)y\sinh(\alpha y) \\ g(x,y,t) = \phi_5(x,t)\cosh(\alpha y) + \phi_6(x,t)\sinh(\alpha y) + \phi_7(x,t)y\cosh(\alpha y) + \phi_8(x,t)y\sinh(\alpha y) \end{array} \right. \tag{46}$$

where parameter α has been given an optimal value (namely $\alpha = \frac{\pi}{20}\ mm^{-1}$), based upon prior parametric analyses achieved for several geometric and material configurations in [22].

The facings are presumed to be perfectly bonded to the core layer, what enables one to write the following relations accounting for the continuity of the displacements at the top and bottom interfaces:

- **at the upper skin/core interface:**

$$\mathbf{u}^b(x,-h_s,t) = \mathbf{u}^c(x,h_c,t) \implies \left\{ \begin{array}{ll} u^b + h_s\theta^b = & u_0^c + u_1^c\sinh(\frac{\pi h_c}{L}) + \phi_1\cosh(\alpha h_c) + \phi_2\sinh(\alpha h_c) \\ & +\phi_3 h_c\cosh(\alpha h_c) + \phi_4 h_c\sinh(\alpha h_c) \\ v^b = & v_0^c\cosh(\frac{\pi h_c}{L}) + v_1^c h_c + \phi_5\cosh(\alpha h_c) + \phi_6\sinh(\alpha h_c) \\ & +\phi_7 h_c\cosh(\alpha h_c) + \phi_8 h_c\sinh(\alpha h_c) \end{array} \right. \tag{47}$$

- **at the lower skin/core interface:**

$$\mathbf{u}^a(x,h_s,t) = \mathbf{u}^c(x,-h_c,t) \implies \left\{ \begin{array}{ll} u^a - h_s\theta^a = & u_0^c - u_1^c\sinh(\frac{\pi h_c}{L}) + \phi_1\cosh(\alpha h_c) - \phi_2\sinh(\alpha h_c) \\ & -\phi_3 h_c\cosh(\alpha h_c) + \phi_4 h_c\sinh(\alpha h_c) \\ v^a = & v_0^c\cosh(\frac{\pi h_c}{L}) - v_1^c h_c + \phi_5\cosh(\alpha h_c) - \phi_6\sinh(\alpha h_c) \\ & -\phi_7 h_c\cosh(\alpha h_c) + \phi_8 h_c\sinh(\alpha h_c) \end{array} \right. \tag{48}$$

Taking into consideration the aforementioned displacement continuity constraints, one can rewrite ϕ_1, ϕ_2, ϕ_5 and ϕ_6 in terms of the remaining variables as follows:

$$\begin{array}{l} \phi_1 = \frac{1}{\cosh(\alpha h_c)}\left(\frac{1}{2}(u^b+u^a) + \frac{h_s}{2}(\theta^b-\theta^a) - u_0^c - \phi_4 h_c\sinh(\alpha h_c)\right) \\ \phi_2 = \frac{1}{\sinh(\alpha h_c)}\left(\frac{1}{2}(u^b-u^a) + \frac{h_s}{2}(\theta^b+\theta^a) - u_1^c\sinh(\frac{\pi h_c}{L}) - \phi_3 h_c\cosh(\alpha h_c)\right) \\ \phi_5 = \frac{1}{\cosh(\alpha h_c)}\left(\frac{1}{2}(v^b+v^a) - v_0^c\cosh(\frac{\pi h_c}{L}) - \phi_8 h_c\sinh(\alpha h_c)\right) \\ \phi_6 = \frac{1}{\sinh(\alpha h_c)}\left(\frac{1}{2}(v^b-v^a) - v_1^c h_c - \phi_7 h_c\cosh(\alpha h_c)\right) \end{array} \tag{49}$$

reducing thus the total number of fundamental kinematic unknowns to 14 for the whole sandwich, which can be brought together in a unique vector:

$$\mathbf{d}(x,t) = \left\langle u^b \; u^a \; v^b \; v^a \; \theta^b \; \theta^a \; u_1^c \; v_0^c \; \phi_3 \; \phi_4 \; \phi_7 \; \phi_8 \; u_0^c \; v_1^c \right\rangle^T \tag{50}$$

Finally, the strain-displacement relationship in the core layer simply writes:

$$\boldsymbol{\varepsilon}^c = \frac{1}{2}(\nabla \mathbf{u}^c + \nabla^T \mathbf{u}^c) \tag{51}$$

where the (in-plane) components of the displacement gradient tensor can be found in [22, 23].

Thereafter, the 3D stress-strain constitutive law in the foam core:

$$\boldsymbol{\sigma}^c = \lambda_c tr(\boldsymbol{\varepsilon}^c)\mathbf{I} + 2\mu_c \boldsymbol{\varepsilon}^c \tag{52}$$

comes down to the following reduced expression, according to the plane stress hypothesis:

$$\mathbf{s}_c = \left\{ \begin{array}{c} \sigma_{xx}^c \\ \sigma_{yy}^c \\ \sigma_{xy}^c \end{array} \right\} = \left[\begin{array}{ccc} \lambda_c^* + 2\mu_c & \lambda_c^* & 0 \\ \lambda_c^* & \lambda_c^* + 2\mu_c & 0 \\ 0 & 0 & \mu_c \end{array} \right] \left\{ \begin{array}{c} \varepsilon_{xx}^c \\ \varepsilon_{yy}^c \\ 2\varepsilon_{xy}^c \end{array} \right\} = \mathbf{L}_c \boldsymbol{\gamma}_c \tag{53}$$

3.2. Virtual work principle

The governing equations of the problem are derived here from the principle of virtual work. The following relation holds for any kinematically admissible displacement variation $\delta\mathbf{u}$:

$$\delta\mathcal{A}(\delta\mathbf{u}) = \delta\mathcal{W}_{int}(\delta\mathbf{u}) + \delta\mathcal{W}_{ext}(\delta\mathbf{u}) \tag{54}$$

On one hand, the virtual work of the internal forces $\delta\mathcal{W}_{int}$ takes the following form:

$$\begin{array}{rcl} \delta\mathcal{W}_{int} & = & -\sum_{i=a,b,c} \int_{\Omega_i} \boldsymbol{\sigma}^i : \delta\boldsymbol{\varepsilon}^i \mathrm{d}\Omega_i \\ & = & -\int_0^L \left(\int_{-h_s}^{h_s} \left(\sigma_{xx}^a \delta\varepsilon_{xx}^a + 2\sigma_{xy}^a \delta\varepsilon_{xy}^a \right) \mathrm{d}y + \int_{-h_c}^{h_c} \left(\sigma_{xx}^c \delta\varepsilon_{xx}^c + \sigma_{yy}^c \delta\varepsilon_{yy}^c + 2\sigma_{xy}^c \delta\varepsilon_{xy}^c \right) \mathrm{d}y \right. \\ & & \left. + \int_{-h_s}^{h_s} \left(\sigma_{xx}^b \delta\varepsilon_{xx}^b + 2\sigma_{xy}^b \delta\varepsilon_{xy}^b \right) \mathrm{d}y \right) \mathrm{d}x \end{array} \tag{55}$$

whereas the external virtual work $\delta\mathcal{W}_{ext}$ can be simply ignored in the context of free vibrations.

On the other hand, the virtual work of the acceleration quantities $\delta\mathcal{A}$ writes:

$$\delta\mathcal{A} = \int_{\Omega_a} \delta\mathbf{u}^a . \rho_s \ddot{\mathbf{u}}^a \mathrm{d}\Omega_a + \int_{\Omega_c} \delta\mathbf{u}^c . \rho_c \ddot{\mathbf{u}}^c \mathrm{d}\Omega_c + \int_{\Omega_b} \delta\mathbf{u}^b . \rho_s \ddot{\mathbf{u}}^b \mathrm{d}\Omega_b \tag{56}$$

Let us now introduce the following vector of generalized displacements (where functions ϕ_1, ϕ_2, ϕ_5 and ϕ_6 and their derivatives have been discarded, due to the continuity conditions):

$$\begin{array}{rl} \mathbf{q}(x,t) = & \left\langle u^b \; u^a \; u,_x^b \; u,_x^a \; v^b \; v^a \; v,_x^b \; v,_x^a \; \theta^b \; \theta^a \; \theta,_x^b \; \theta,_x^a \; u_1^c \; u_1,_x^c \; v_0^c \; v_0,_x^c \right. \\ & \left. \phi_3 \; \phi_4 \; \phi_7 \; \phi_8 \; \phi_3,_x \; \phi_4,_x \; \phi_7,_x \; \phi_8,_x \; u_0^c \; u_0,_x^c \; v_1^c \; v_1,_x^c \right\rangle^T \end{array} \tag{57}$$

and the matrices $\mathbf{H}_a$, $\mathbf{H}_b$ and $\mathbf{H}_c$ (whose non-zero components can also be found in [22, 23]) such that:

$$\boldsymbol{\gamma}_i = \mathbf{H}_i \mathbf{q} \qquad (i = a, b, c) \tag{58}$$

Let us also introduce the matrices $\mathbf{P}_a$, $\mathbf{P}_b$ and $\mathbf{P}_c$ (whose non-zero components are reported in Appendix A), which relate the vector of unknown displacements to the displacement vectors in each layer as follows:

$$\mathbf{u}^i = \mathbf{P}_i \mathbf{d} \qquad (i = a, b, c) \tag{59}$$

Equations (55) and (56) can then be rewritten in the following form:

$$\begin{aligned}
\delta \mathcal{W}_{int} &= -\int_0^L \left(\int_{-h_s}^{h_s} \delta \boldsymbol{\gamma}_a^T \mathbf{s}_a \mathrm{d}y + \int_{-h_s}^{h_s} \delta \boldsymbol{\gamma}_b^T \mathbf{s}_b \mathrm{d}y + \int_{-h_c}^{h_c} \delta \boldsymbol{\gamma}_c^T \mathbf{s}_c \mathrm{d}y \right) \mathrm{d}x \\
&= -\int_0^L \left(\int_{-h_s}^{h_s} \delta \mathbf{q}^T \mathbf{H}_a^T \mathbf{L}_s \mathbf{H}_a \mathbf{q} \mathrm{d}y + \int_{-h_s}^{h_s} \delta \mathbf{q}^T \mathbf{H}_b^T \mathbf{L}_s \mathbf{H}_b \mathbf{q} \mathrm{d}y + \int_{-h_c}^{h_c} \delta \mathbf{q}^T \mathbf{H}_c^T \mathbf{L}_c \mathbf{H}_c \mathbf{q} \mathrm{d}y \right) \mathrm{d}x \\
\delta \mathcal{A} &= -\int_0^L \left(\int_{-h_s}^{h_s} \delta \mathbf{d}^T \mathbf{P}_a^T \rho_s \mathbf{P}_a \ddot{\mathbf{d}} \mathrm{d}y + \int_{-h_s}^{h_s} \delta \mathbf{d}^T \mathbf{P}_b^T \rho_s \mathbf{P}_b \ddot{\mathbf{d}} \mathrm{d}y + \int_{-h_c}^{h_c} \delta \mathbf{d}^T \mathbf{P}_c^T \rho_c \mathbf{P}_c \ddot{\mathbf{d}} \mathrm{d}y \right) \mathrm{d}x
\end{aligned} \tag{60}$$

It should be mentioned that the integrations with respect to the y-coordinate are performed analytically through the thickness of the skins (introducing a shear correction factor of $\frac{5}{6}$ in the resulting shear quantities, as for homogeneous beams, according to the Timoshenko beam theory), while numerical integrations using Gaussian quadratures are carried out through the core thickness as it involves more complex hyperbolic functions.

3.3. Finite element discretization

The problem is now discretized using 3-node isoparametric elements with quadratic shape functions (see Figure 2).

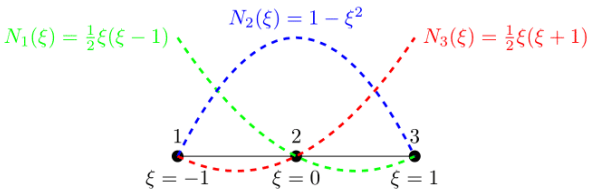


Figure 2: Graphical representation of the interpolation functions of the 3-node reference 1D element

Within a given finite element e, all the components of vector $\mathbf{d}$ are interpolated in the same way, introducing the elementary nodal displacement vector $\mathbf{D}^e$ composed of the 42 degrees of freedom of the given element and the associated interpolation matrix $\mathbf{N}$:

$$\mathbf{d} = \mathbf{N}\mathbf{D}^e \tag{61}$$

with $\mathbf{D}^e = \left\langle \mathbf{D}_1^{e^T} \ \mathbf{D}_2^{e^T} \ \mathbf{D}_3^{e^T} \right\rangle^T$, where $\mathbf{D}_i^e \triangleq \mathbf{d}(x_i) = \left\langle u^b \ u^a \ v^b \ v^a \ \theta^b \ \theta^a \ u_1^c \ v_0^c \ \phi_3 \ \phi_4 \ \phi_7 \ \phi_8 \ u_0^c \ v_1^c \right\rangle_i^T$ contains the 14 degrees of freedom of the i-th node of element e.

Finally, the generalized displacement vector $\mathbf{q}$ may be expressed in terms of $\mathbf{d}$ (by means of a transformation matrix $\mathbf{T}$ including differential operators) and subsequently in terms of $\mathbf{D}^e$ as follows:

$$\mathbf{q} = \mathbf{T}\mathbf{d} = \mathbf{T}\mathbf{N}\mathbf{D}^e \triangleq \mathbf{G}\mathbf{D}^e \tag{62}$$

According to all these definitions, Equation (54) can be rewritten in the following discretized form:

$$\begin{array}{c} \sum_e \int_{-1}^{1} \delta\mathbf{D}^{e^T} \left(\int_{-h_s}^{h_s} \mathbf{C}_a^T \rho_s \mathbf{C}_a \mathrm{d}y + \int_{-h_s}^{h_s} \mathbf{C}_b^T \rho_s \mathbf{C}_b \mathrm{d}y + \int_{-h_c}^{h_c} \mathbf{C}_c^T \rho_c \mathbf{C}_c \mathrm{d}y \right) \ddot{\mathbf{D}}^e \frac{L_e}{2} \mathrm{d}\xi \\ + \sum_e \int_{-1}^{1} \delta\mathbf{D}^{e^T} \left(\int_{-h_s}^{h_s} \mathbf{B}_a^T \mathbf{L}_s \mathbf{B}_a \mathrm{d}y + \int_{-h_s}^{h_s} \mathbf{B}_b^T \mathbf{L}_s \mathbf{B}_b \mathrm{d}y + \int_{-h_c}^{h_c} \mathbf{B}_c^T \mathbf{L}_c \mathbf{B}_c \mathrm{d}y \right) \mathbf{D}^e \frac{L_e}{2} \mathrm{d}\xi \\ = \sum_e \delta\mathbf{D}^{e^T} \mathbf{M}^e \ddot{\mathbf{D}}^e + \sum_e \delta\mathbf{D}^{e^T} \mathbf{K}^e \mathbf{D}^e = 0 \end{array} \tag{63}$$

where:

$$\mathbf{C}_i = \mathbf{P}_i \mathbf{N} \qquad \mathbf{B}_i = \mathbf{H}_i \mathbf{G} \qquad (i = a, b, c) \tag{64}$$

and $\mathbf{M}^e$ and $\mathbf{K}^e$ represent the elementary mass and stiffness matrices. In Equation (63), the integration over a real element is replaced by the integration over the reference element by means of the following variable change: $\mathrm{d}x = \frac{L_e}{2}\mathrm{d}\xi$ (L_e being the elementary length). A reduced numerical integration scheme (with 2 Gaussian points by element) is employed so as to prevent from any shear-locking phenomenon.

The free vibration problem can ultimately be expressed as follows:

$$\mathbf{M}\ddot{\mathbf{D}} + \mathbf{K}\mathbf{D} = \mathbf{0} \tag{65}$$

where matrices $\mathbf{M}$ and $\mathbf{K}$ are assembled from elementary matrices, according to the definition of the global nodal displacement vector $\mathbf{D}$. Inserting $\mathbf{D} = \mathbf{X}e^{\mathrm{i}\omega t}$ in Equation (65) allows one to derive the natural frequencies and corresponding vibration modes as the eigenvalues and eigenvectors of the algebraic equation system:

$$(\mathbf{K} - \omega^2 \mathbf{M})\mathbf{X} = \mathbf{0} \tag{66}$$

The new mass matrix $\mathbf{M}$ of the 1D enriched finite element has been implemented, in addition to the stiffness matrix $\mathbf{K}$ already present, in the home-made program previously developed in the context of buckling analyses. The natural frequencies and the associated modes of the sandwich column can be then calculated by the use of a QZ algorithm through a standard Fortran subroutine from the EISPACK package [24] devoted to generalized eigenvalue problems.

4. Results and validation

4.1. Numerical simulation of the natural frequencies and vibration modes using Abaqus

Two-dimensional numerical finite element computations (linearized frequency analyses) have been performed using Abaqus software, in order to validate the previous analytical and numerical solutions. For this purpose, a 2D geometry of the sandwich column is retained, where both the foam core and the two skins

are represented by a 2D continuous solid satisfying the plane stress condition. The associated finite element mesh is made up of 8-node quadrangular elements with reduced integration. After a few preliminary convergence analyses, the same mesh is retained for all the calculations, displaying 100 elements along the length, 10 elements in the thickness of the foam core and 2 elements in the thickness of each skin (accordingly, 100 elements will be also considered along the length of the sandwich structure in the subsequent computations involving the 1D finite element model).

4.2. Verification of the analytical solutions

Firstly, let us consider the case of guided boundary conditions which was solved analytically. Under these conditions, the vibration modes are shown to display sinusoidal variations along the length. Two cases are encountered, depending on whether the sinusoidal deformed shapes of the skins are in phase or in phase opposition, giving rise to so-called antisymmetric and symmetric modes. In the sequel, the analytical solutions are compared to both 1D and 2D numerical results obtained with the home-made program and Abaqus software, respectively. In the 1D finite element model, guided boundary conditions are enforced by setting to zero the following degrees of freedom at both ends of the beam: u^b, u^a, θ^b, θ^a, u_1^c, ϕ_3, ϕ_4 and u_0^c; whereas in the 2D numerical model, the longitudinal displacement of the core and the two skin layers is prohibited at both ends. Let us note that, during both numerical computations (with the 1D model as well as the 2D model), when the displacement boundary conditions are appropriately enforced at both ends as described above, a rigid mode is first encountered, corresponding to an overall movement of the sandwich column in the transverse direction. This rigid mode can be viewed as a particular antisymmetric mode but it will be naturally discarded as the corresponding eigenfrequency is plainly null. The geometric and material parameters considered in all the subsequent analyses, listed in Table 1, are retrieved from previous papers from the authors dealing with sandwich buckling and post-buckling. Let us mention that a few parametric analyses have been performed in this study, which will not be presented in the current paper for conciseness purposes. The geometry of the sandwich structure and the material properties obviously influence the natural frequencies, but in all practical cases, similar significant features are observed and the same conclusions can be drawn. Consequently, a single geometric and material configuration will be considered in the sequel, with a particularly thick and soft core layer, so as to reveal at best the benefits of the present analytical and numerical developments.

$E_s\ (MPa)$	$E_c\ (MPa)$	ν_s	ν_c	$\rho_s\ (kg/m^3)$	$\rho_c\ (kg/m^3)$	$L\ (mm)$	$h_s\ (mm)$	$h_c\ (mm)$
70000	10	0.3	0.01	2700	60	600	1	60

Table 1: Material and geometric parameters

In Figure 3, the first natural frequencies ($f = \frac{\omega}{2\pi}$ in Hz) are plotted versus the half-wave number of the

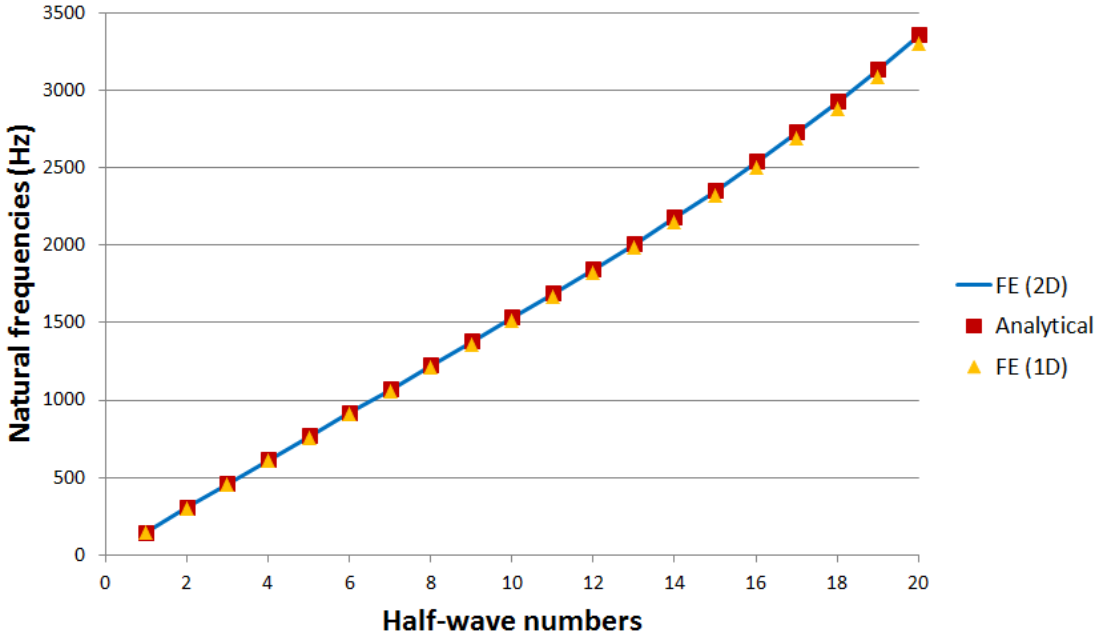
corresponding modes, in both cases of antisymmetric and symmetric modes. The results generally show a very good agreement between analytical and numerical values. In particular, the order of appearance of the successive modes is perfectly similar between the three approaches.

In the antisymmetric case, the frequency regularly increases with the wave number, in such a way that the first mode (associated with the minimum eigenfrequency) displays only one single sinusoidal half wave along the length. Conversely, when dealing with symmetric modes, on one side, the natural frequencies seem to keep almost constant for small wave numbers (say $n < 5$ in the present case), including the case of a null wave number, corresponding to a uniform transverse tension-compression of the foam core without deformation of the skins. This constant value is found to be larger than the eigenfrequencies of antisymmetric modes with the same wave numbers. Then, from a particular threshold wave number, some of the modes are found in pairs (see Figure 4): for each given wave number that is sufficiently large, two modes occur (one being antisymmetric and the other symmetric) with almost the same natural frequency. The eigenfrequency corresponding to the antisymmetric mode is always slightly lower than the one associated with the symmetric mode, but the two values practically coincide from a certain point. It can be shown that the threshold value of the wave number from which antisymmetric and symmetric modes share the same natural frequencies is directly related to the ratio between the thickness of the core layer and the wavelength of the mode. When this ratio is particularly high, the two faces are found to vibrate in an uncoupled way (there is no interaction between them), so that they can equally be in phase or in phase opposition without changing the corresponding oscillation frequency (the relative sign of the eigenmode component of each face, determining the antisymmetric or symmetric nature of the overall vibration mode, has no influence on the natural frequency).

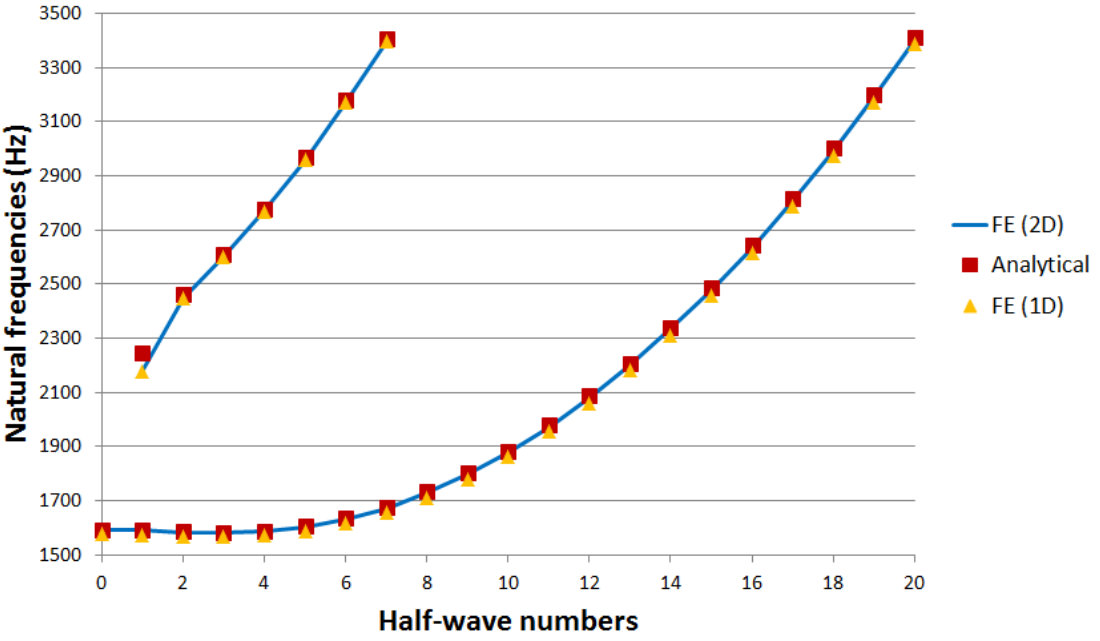
On the other side, a second type of symmetric modes is also encountered, as plotted in Figure 3(b), with higher natural frequencies. It means that, for each wave number ($n \geqslant 1$), two different symmetric modes are observed, with completely different eigenfrequencies. The associated eigenmodes are similar, as long as the sinusoidal deformed shape of the skins is concerned, but the modal deformation of the core layer strongly differs between them, as is illustrated in Figure 5 for a particular wave number. All these results demonstrate that the present analytical and numerical formulations are capable of capturing very accurately the displacement fields inside the core layer, contrary to more classical (even higher-order) beam models with more approximate kinematics.

4.3. Verification of the 1D numerical model

In order to verify further the 1D finite element model presented above, a new case is considered with the same geometric and material parameters as before (see Table 1), but new boundary conditions. The choice



(a) Antisymmetric modes



(b) Symmetric modes

Figure 3: Natural frequencies of the sandwich column with guided boundary conditions

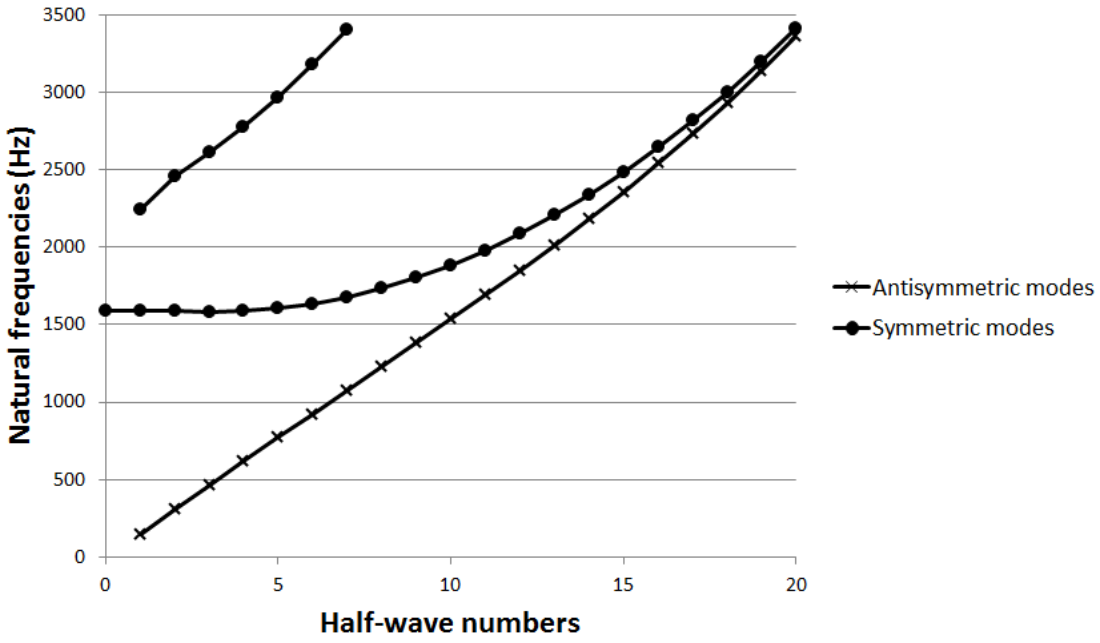
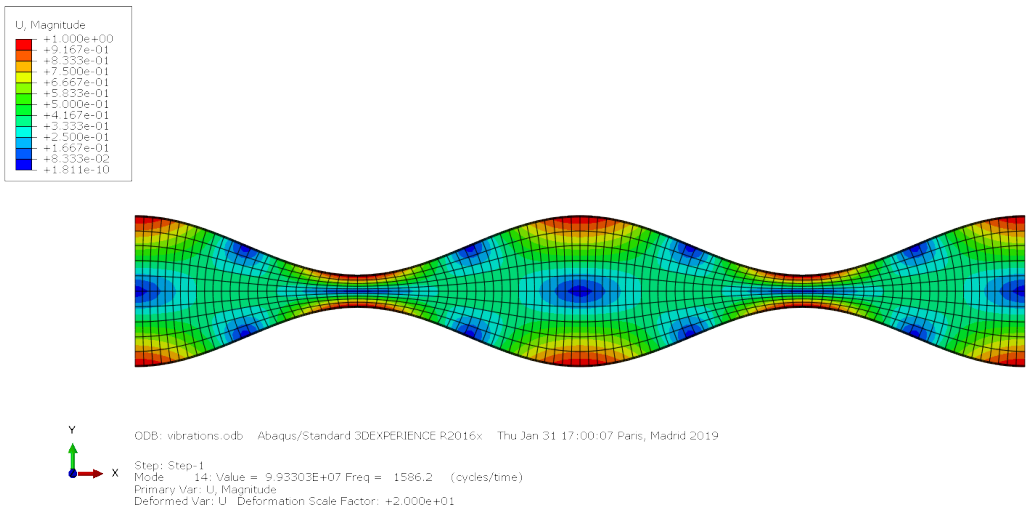


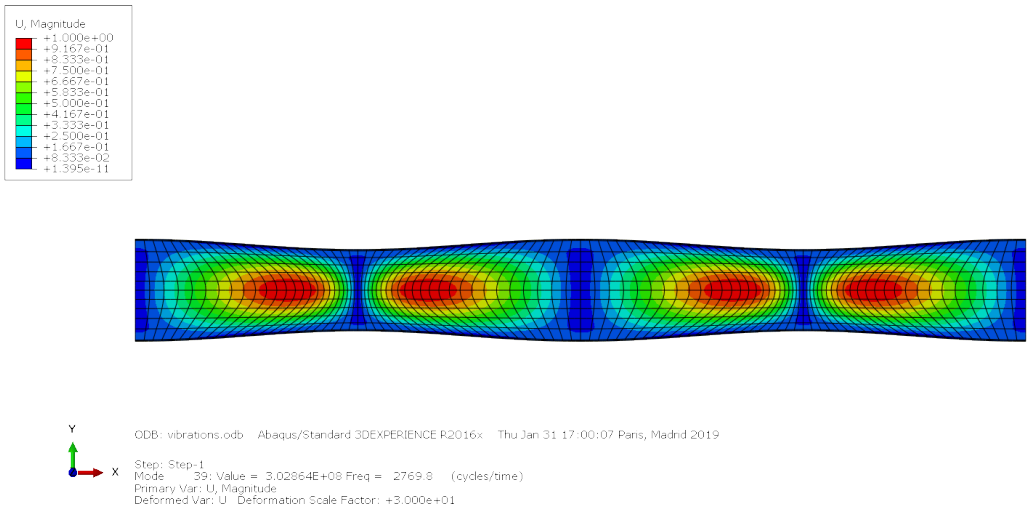
Figure 4: Comparison between natural frequencies of antisymmetric and symmetric modes

of free boundary conditions allows one to obtain more complicated vibration modes that are not expected to be derived analytically. Again, the natural frequencies obtained with the present 1D model are compared to the ones resulting from 2D finite element computations using Abaqus. Both are plotted in Figure 6 versus the mode number (the first three rigid modes are once more discarded). A very good general agreement is still achieved between the two approaches. However, while a perfect match is reached for the first quasi-sinusoidal modes (as well as in the previous case of guided boundary conditions and sinusoidal modes), the concordance is a little bit less pronounced, as soon as more complex modes are concerned. It is naturally due to the fact that the shape functions used in the definition of the kinematics along the transverse direction of the core layer turn out to be similar to the analytical solutions obtained in the case of guided ends and thus sinusoidal longitudinal deformed shapes. Nevertheless, the relative error between the natural frequencies never exceeds 5% at the maximum.

Eventually, some remarkable modes are depicted in Figures 7, 8, 9 and 10, for illustration and validation purposes, which are typically obtained here in the case of free boundary conditions, since there are no kinematic limitations at both ends of the sandwich beam. All the modal deformed shapes resulting from the 1D model have been rebuilt as follows: the deformed mid-lines of the upper and lower skins have been represented using the appropriate displacement fields $u^b(x)$, $v^b(x)$, $u^a(x)$ and $v^a(x)$, respectively, while the deformed shape of the foam core has been plotted in the form of contour lines, using the displacement



(a) First symmetric mode ($f = 1586\ Hz$)



(b) Second symmetric mode ($f = 2770\ Hz$)

Figure 5: Two different symmetric modes with the same wave number ($n = 4$)

expressions (45) as functions of the y-coordinate and the kinematic fields $u_0^c(x)$, $u_1^c(x)$, $v_0^c(x)$, $v_1^c(x)$, $\phi_1(x)$, $\phi_2(x)$, $\phi_3(x)$, $\phi_4(x)$, $\phi_5(x)$, $\phi_6(x)$, $\phi_7(x)$ and $\phi_8(x)$. It shows again the reliability of the present 1D model in the derivation of any natural frequency and vibration mode of the sandwich column, whatever the considered boundary conditions.

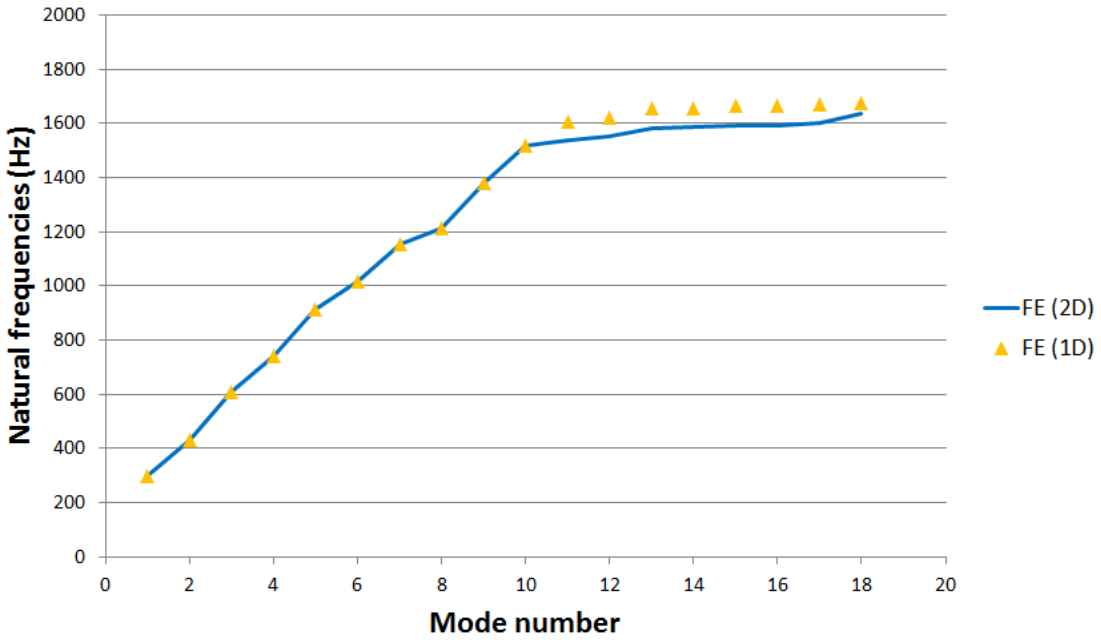
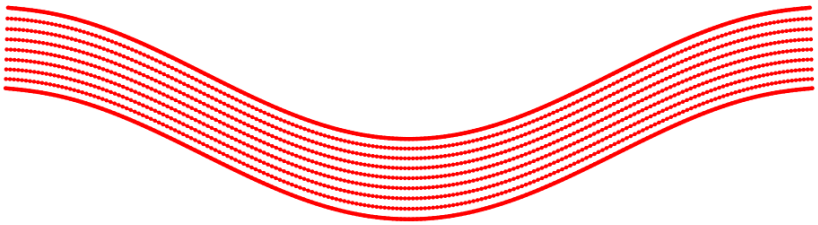


Figure 6: Natural frequencies of the sandwich column with free boundary conditions

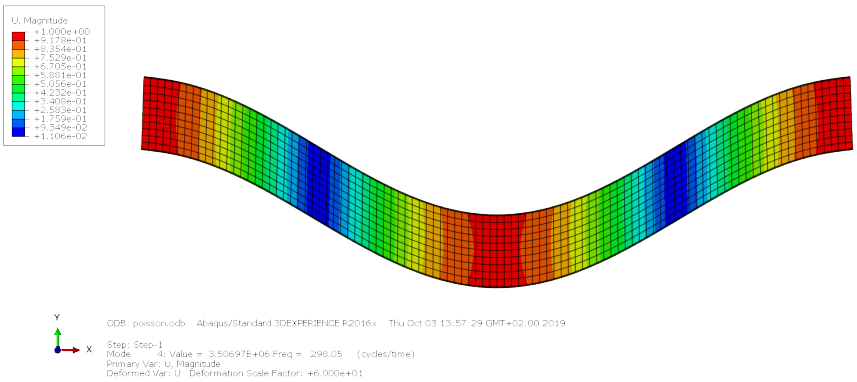
5. Conclusions

The free vibration problem of a sandwich column has been investigated in this paper. Analytical solutions were first obtained for the natural frequencies and corresponding vibration modes, based on the use of Hamilton's principle. The two identical skins were modeled as Euler-Bernoulli beams, whereas the core layer was considered as a 2D solid continuous medium, without any presupposed kinematics. The eigenvalue problem in hand leads to a system of partial differential equations which are solved together with a particular set of standard boundary conditions, that allows one to derive partially explicit forms of the eigenmodes and the eigenfrequencies as solutions of a transcendental equation.

Furthermore, a 1D enriched "sandwich" finite element model has been developed so as to deal with more complex configurations such as more general boundary conditions. This model has already been instigated in the context of buckling and post-buckling analyses in previous studies from some of the authors. Here, restricting oneself to a geometrically and materially linear framework, emphasis is given to the inertial terms in the formulation and to the construction of the mass matrix of this special finite element. In the numerical model, the skins are described as Timoshenko beams including possible transverse shear effects, in such a way that there is no particular restriction on their thickness. Besides, the displacement field variation through the thickness of the core layer relies on real deformation shapes (namely hyperbolic functions) obtained analytically when considering sinusoidal modal solutions in the longitudinal direction. The resulting formulation gives an accurate representation of the general displacement field throughout the



(a) Mode 1 with 1D model ($f = 298\ Hz$)

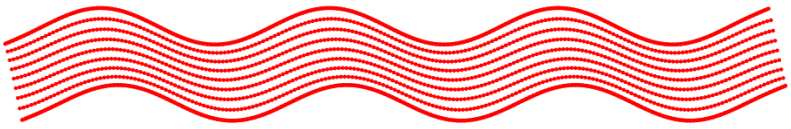


(b) Mode 1 with 2D model ($f = 298\ Hz$)

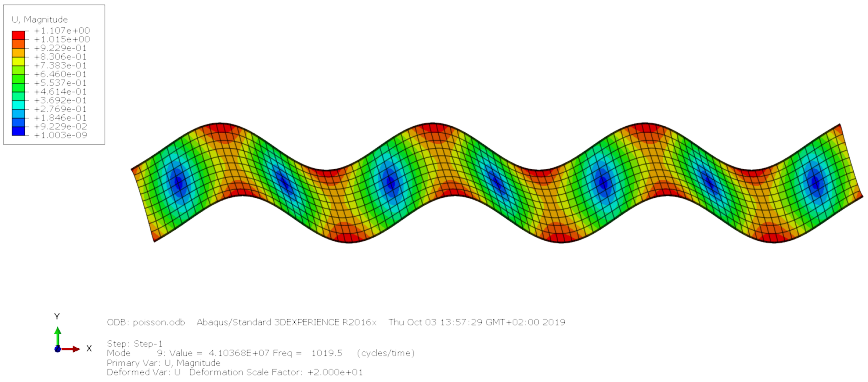
Figure 7: Comparison of vibration modes obtained with the 1D and 2D numerical models with free ends

sandwich column by means of a set of 14 unknown fields only depending on the longitudinal coordinate. The structure is then discretized using 3-node Lagrangian 1D elements with 14 degrees of freedom per node, and the generalized eigenvalue problem of free vibrations is numerically solved so as to derive the natural frequencies and associated modes of the sandwich column.

The numerical results derived from this computationally efficient 1D model were compared to 2D finite element reference results performed using Abaqus software for validation purposes, and also to the previous analytical solutions once the appropriate boundary conditions are considered. All the results are in very good agreement, all the more so when the modes brought into play are sinusoidal in the longitudinal direction, but also for any other boundary conditions where the skins deform in any other way (with less than 5% of relative error). As far as sinusoidal modes are concerned, it is shown that antisymmetric modes are invariably obtained before symmetric modes, namely for lower eigenfrequencies. However, when considering sufficiently high wave numbers, both antisymmetric and symmetric modes tend to coincide in terms of natural frequency.



(a) Mode 6 with 1D model ($f = 1019\ Hz$)



(b) Mode 6 with 2D model ($f = 1019\ Hz$)

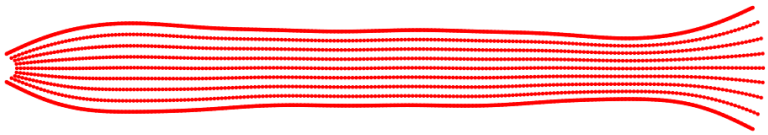
Figure 8: Comparison of vibration modes obtained with the 1D and 2D numerical models with free ends

Lastly, for each wave number, while one single antisymmetric mode is observed, two different symmetric modes can be identified. The first one almost coincides to the corresponding antisymmetric mode in terms of natural frequency, as soon as the wave number is sufficiently high (as if the vibrations of the two skins were uncoupled). Conversely, the second one displays a greater eigenfrequency due to the more energy-consuming modal deformation shape of the core material. This original result is specifically obtained thanks to a rigorous description of the deformation field in the core layer, in both present analytical and numerical modeling approaches.

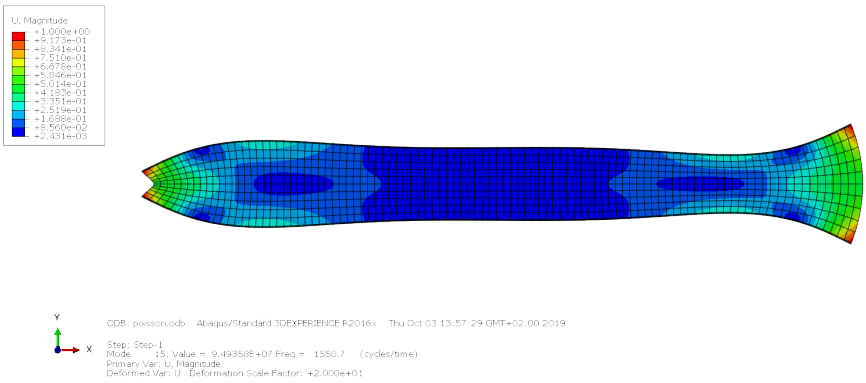
This 1D finite element model, and particularly the previous non-linear developments performed in the context of post-buckling analyses combined to the present introduction of inertial effects, is likely to deal with further non-linear dynamic problems involving modal interactions.

Data availability statement

The raw/processed data required to reproduce these findings cannot be shared at this time as the data also forms part of an ongoing study.



(a) Mode 12 with 1D model ($f = 1621\ Hz$)



(b) Mode 12 with 2D model ($f = 1551\ Hz$)

Figure 9: Comparison of vibration modes obtained with the 1D and 2D numerical models with free ends

Declaration of Competing Interests

The authors declare that they have no known competing financial interests or personal relationships that could have appeared to influence the work reported in this paper.

References

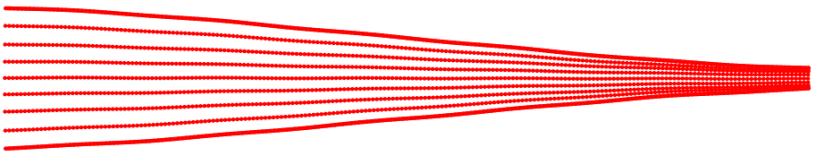
[1] Reddy, J.N., An evaluation of equivalent-single-layer and layerwise theories of composite laminates, *Composite Structures* **25** Issues 1-4 (1993) 21–35.

[2] Carrera, E., Theories and finite elements for multilayered, anisotropic, composite plates and shells, *Archives of Computational Methods in Engineering* **9** Issue 2 (2002) 87–140.

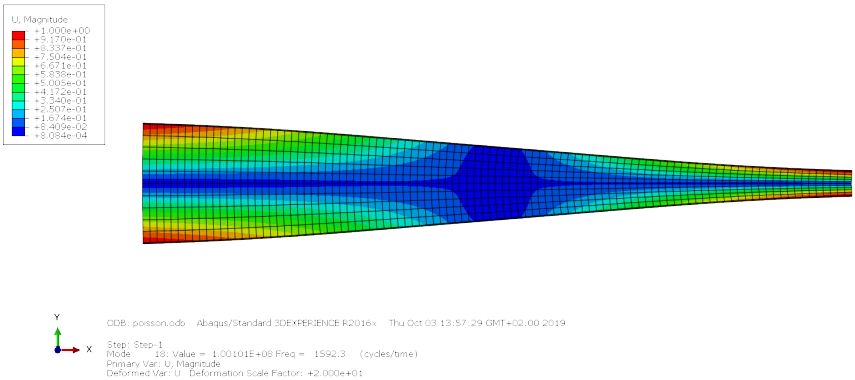
[3] Carrera, E., Theories and finite elements for multilayered plates and shells: a unified compact formulation with numerical assessment and benchmarking, *Archives of Computational Methods in Engineering* **10** Issue 3 (2003) 215–296.

[4] Demasi, L., ∞^6 Mixed plate theories based on the Generalized Unified Formulation. Part II: Layerwise theories, *Composite Structures* **87** Issue 1 (2009) 12–22.

[5] Liu, D. and Li, X., An overall view of laminate theories based on displacement hypothesis, *Journal of Composite Materials* **30** Issue 14 (1996) 1539–1561.



(a) Mode 15 with 1D model ($f = 1664\ Hz$)



(b) Mode 15 with 2D model ($f = 1592\ Hz$)

Figure 10: Comparison of vibration modes obtained with the 1D and 2D numerical models with free ends

[6] Ghugal, Y.M. and Shimpi, R.P., A review of refined shear deformation theories of isotropic and anisotropic laminated plates, *Journal of Reinforced Plastics and Composites* **21** Issue 9 (2002) 775–813.

[7] Zhen, W. and Wanji, C., An assessment of several displacement-based theories for the vibration and stability analysis of laminated composite and sandwich beams, *Composite Structures* **84** Issue 4 (2008) 337–349.

[8] Hu, H., Belouettar, S., Potier-Ferry, M. and Daya, E.M., Review and assessment of various theories for modeling sandwich composites, *Composite Structures* **84** Issue 3 (2008) 282–292.

[9] Phan, C.N., Frostig, Y. and Kardomateas, G.A., Analysis of sandwich beams with a compliant core and with in-plane rigidity – Extended high-order sandwich panel theory versus elasticity, *Journal of Applied Mechanics* **79** (2012) 1–11.

[10] Phan, C.N., Bailey, N.W., Kardomateas, G.A. and Battley, M.A., Wrinkling of sandwich wide panels/beams based on the extended high-order sandwich panel theory: formulation, comparison with elasticity and experiments, *Archive of Applied Mechanics* **82** Issues 10-11 (2012) 1585–1599.

[11] Allen, H.G., *Analysis and Design of Structural Sandwich Panels* (Pergamon, 1969).

[12] Benson, A.S. and Mayers, J., General instability and face wrinkling of sandwich plates: Unified theory and applications, *AIAA Journal* **5** Issue 4 (1967) 729–739.

[13] Sakiyama, T., Matsuda, H. and Morita, C., Free vibration analysis of sandwich beam with elastic or viscoelastic core by applying the discrete Green function, *Journal of Sound and Vibration* **191** Issue 2 (1996) 189–206.

[14] Banerjee, J.R. and Sobey, A.J., Dynamic stiffness formulation and free vibration analysis of a three-layered sandwich beam, *International Journal of Solids and Structures* **42** Issue 8 (2005) 2181–2197.

[15] Banerjee, J.R., Cheung, C.W., Morishima, R., Perera, M. and Njuguna, J., Free vibration of a three-layered sandwich

beam using the dynamic stiffness method and experiment, *International Journal of Solids and Structures* **44** Issues 22-23 (2007) 7543–7563.

[16] Lou, J., Ma, L. and Wu, L., Free vibration analysis of simply supported sandwich beams with lattice truss core, *Materials Science and Engineering B* **177** Issue 19 (2012) 1712–1716.

[17] Kant, T. and Swaminathan, K., Analytical solutions for free vibration of laminated composite and sandwich plates based on a higher-order refined theory, *Composite Structures* **53** Issue 1 (2001) 73–85.

[18] Arvin, H., Sadighi, M. and Ohadi, A.R., A numerical study of free and forced vibration of composite sandwich beam with viscoelastic core, *Composite Structures* **92** Issue 4 (2010) 996–1008.

[19] Wang, Y. and Wang, X., Free vibration analysis of soft-core sandwich beams by the novel weak form quadrature element method, *Journal of Sandwich Structures and Materials* **18** Issue 3 (2016) 294–320.

[20] Wang, X. and Liang, X., Free vibration of soft-core sandwich panels with general boundary conditions by harmonic quadratic element method, *Thin-Walled Structures* **113** (2017) 253–261.

[21] Douville, M.A. and Le Grognec, P., Exact analytical solutions for the local and global buckling of sandwich beam-columns under various loadings, *International Journal of Solids and Structures* **50** Issues 16-17 (2013) 2597–2609.

[22] Sad Saoud, K. and Le Grognec, P., An enriched 1D finite element for the buckling analysis of sandwich beam-columns, *Computational Mechanics* **57** Issue 6 (2016) 887–900.

[23] Sad Saoud, K. and Le Grognec, P., Post-buckling analysis of elastoplastic sandwich columns by means of an enriched 1D finite element model, *International Journal of Solids and Structures* **129** (2017) 90–102.

[24] Smith, B.T., Boyle, J.M., Dongarra, J.J., Garbow, B.S., Ikebe, Y., Klema, V.C. and Moler, C.B., *Matrix eigensystem routines – EISPACK guide* (Springer, 1976).

Appendix A. Useful matrices

The non-zero components of matrix $\mathbf{P}_a$ are:

$$P_a(1,2) = 1 \qquad P_a(1,6) = -y \qquad P_a(2,4) = 1 \tag{A.1}$$

The non-zero components of matrix $\mathbf{P}_b$ are:

$$P_b(1,1) = 1 \qquad P_b(1,5) = -y \qquad P_b(2,3) = 1 \tag{A.2}$$

The non-zero components of matrix $\mathbf{P}_c$ are:

$$
\begin{aligned}
P_c(1,1) &= \tfrac{\cosh(\alpha y)}{2\cosh(\alpha h_c)} + \tfrac{\sinh(\alpha y)}{2\sinh(\alpha h_c)} \\
P_c(1,2) &= \tfrac{\cosh(\alpha y)}{2\cosh(\alpha h_c)} - \tfrac{\sinh(\alpha y)}{2\sinh(\alpha h_c)} \\
P_c(1,5) &= h_s \tfrac{\cosh(\alpha y)}{2\cosh(\alpha h_c)} + h_s \tfrac{\sinh(\alpha y)}{2\sinh(\alpha h_c)} \\
P_c(1,6) &= -h_s \tfrac{\cosh(\alpha y)}{2\cosh(\alpha h_c)} + h_s \tfrac{\sinh(\alpha y)}{2\sinh(\alpha h_c)} \\
P_c(1,7) &= \sinh(\tfrac{\pi y}{L}) - \sinh(\tfrac{\pi h_c}{L}) \tfrac{\sinh(\alpha y)}{\sinh(\alpha h_c)} \\
P_c(1,9) &= y\cosh(\alpha y) - h_c \cosh(\alpha h_c) \tfrac{\sinh(\alpha y)}{\sinh(\alpha h_c)} \\
P_c(1,10) &= y\sinh(\alpha y) - h_c \sinh(\alpha h_c) \tfrac{\cosh(\alpha y)}{\cosh(\alpha h_c)} \\
P_c(1,13) &= 1 - \tfrac{\cosh(\alpha y)}{\cosh(\alpha h_c)} \\
P_c(2,3) &= \tfrac{\cosh(\alpha y)}{2\cosh(\alpha h_c)} + \tfrac{\sinh(\alpha y)}{2\sinh(\alpha h_c)} \\
P_c(2,4) &= \tfrac{\cosh(\alpha y)}{2\cosh(\alpha h_c)} - \tfrac{\sinh(\alpha y)}{2\sinh(\alpha h_c)} \\
P_c(2,8) &= \cosh(\tfrac{\pi y}{L}) - \cosh(\tfrac{\pi h_c}{L}) \tfrac{\cosh(\alpha y)}{\cosh(\alpha h_c)} \\
P_c(2,11) &= y\cosh(\alpha y) - h_c \cosh(\alpha h_c) \tfrac{\sinh(\alpha y)}{\sinh(\alpha h_c)} \\
P_c(2,12) &= y\sinh(\alpha y) - h_c \sinh(\alpha h_c) \tfrac{\cosh(\alpha y)}{\cosh(\alpha h_c)} \\
P_c(2,14) &= y - h_c \tfrac{\sinh(\alpha y)}{\sinh(\alpha h_c)}
\end{aligned}
\tag{A.3}
$$